Supporting information

Hollow sp^2-conjugated covalent organic framework encapsulating thiophene-based photosensitizer for enhanced visible-light-driven hydrogen evolution

Chen Yang, Huawei Hu, Cheng Qian, Yaozu Liao*

State Key Laboratory for Modification of Chemical Fibers and Polymer Materials, College of Materials Science and Engineering, Donghua University, Shanghai 201620, China
*Corresponding Author: yzliao@dhu.edu.cn

Table of contents

S1 Experimental Methods

S1.1. Synthesis of pristine COF (g-$C_{18}N_3$-COF)

The synthesis procedure of original COF (g-$C_{18}N_3$-COF) followed the literature with minor modification (**Scheme S1**).[1] A 25 mL pyrex tube was charged with TMTA (61.58 mg, 0.50 mmol), DFB (100.60 mg, 0.75 mmol), KOH (84.15 mg, 1.5 mmol), *n*BuOH (7 mL) and *o*DCB (3 mL), then degassed though with three freeze-pump-thaw cycles (liquid nitrogen bath), sealed under vacuum and sonicated for 5 min. Subsequently, the resulting pale-yellow solution was heated at 120 °C for a 3-day reaction. After cooling to room temperature, the precipitate was collected and washed with methanol, tetrahydrofuran, acetone and dichloromethane in sequence for two times, and then dried under vacuum at 120 °C for 12 h. Finally, pure COF sample was afforded as yellow powder (yield: 88%, relative to the used amount of monomer).

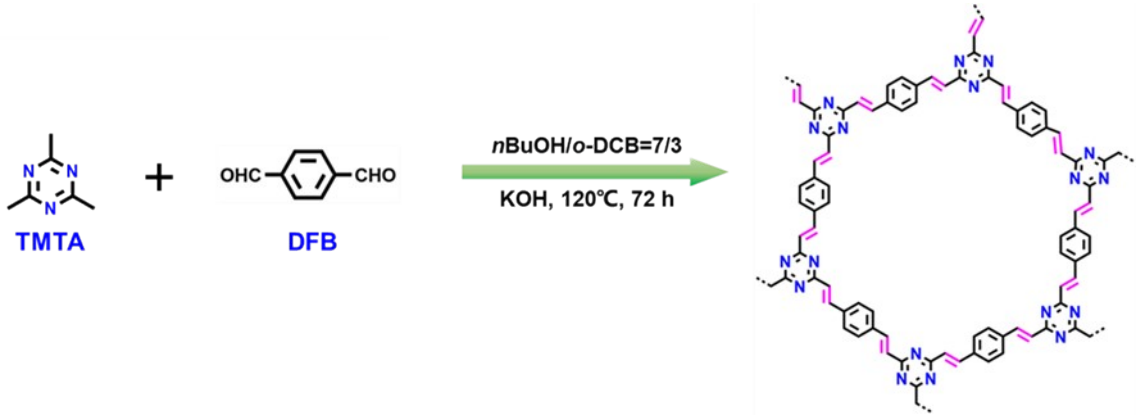

Scheme S1 Synthetic routes for preparing pristine COF via Knoevenagel condensation reaction.

S1.2. Synthesis of g_2T-T

g_2T-T was synthesized according to the reported method. Briefly, the polymerization of g_2T-T was carried out according to the previously reported method, using a Biotage Initiator+ microwave reactor.[2] Specifically, in a dried 5.0 mL microwave vial, 63.8 mg of (3,3‘- bisalkoxy(TEG)-[2,2’-bithiophene]-5,5‘-diyl)bis(trimethylstannane) (155.7 µmol) and 100.0 mg of 5,5’-dibromo-3,3‘-bisalkoxy(TEG)-2,2’-bithiophene (155.7 µmol) were dissolved in 2.0 mL of anhydrous, degassed DMF. $Pd_2(dba)_3$ (2.48 mg, 2.71 µmol) and P(o-tol)$_3$ (3.76 mg, 12.3 µmol) were added and the vial was sealed under nitrogen. The vial was heated under 100℃ for 24 hours. After polymerization, the vial was cooled, 40 µL of 2-(trimethylstannyl)-thiophene was added and the contents were subjected to microwave heating: 2 min 100℃, 2 min 140℃, 2 min 160℃, 2 min 180℃, 5 min 200℃. Finally, 100 µL 2-bromothiophene was added and the reaction was subjected to microwave heating: 2 min 100℃, 2 min 140℃, 2 min 160℃, 2 min 180℃, 5 min 200℃. Then, the reaction mixture was cooled to room temperature and precipitated in methanol. A blue solid was formed, which was filtered into a glass fiberthimble and Soxhlet extraction was carried out with hexane, methanol, ethyl acetate, acetone, and chloroform for 12 h at each step. The polymer dissolved in hot chloroform. Finally, the polymer chloroform solution was concentrated and dried under a high vacuum. A blue solid was obtained with a mass ~80 mg.

S2. Characterization and measurements

The reactions involving inert atmosphere were carried out using standard Schlenk technique. The ^{13}C CP/MAS NMR spectra were taken at a Bruker Advance 400 (400 MHz) spectrometer. X-ray photoelectron spectroscopy (XPS) analyses were determined by a Thermo Escalab 250 Xi spectrometer. Powder X-ray diffraction patterns were recorded on a Bruker D8 Advance diffractometer with Cu-Kα1 radiation (λ = 1.5406 Å). FT-IR spectra were taken on a Thermo Scientific Nicolet iS5 spectrometer. Thermal gravimetric analyses (TGA) were performed on a Libra/209F1 TG-209 thermogravimetric analyzer in nitrogen atmosphere from ambient temperature to 800 °C at the rate of 10 °C min^{-1}. Ultraviolet visible diffuse reflectance spectra (UV-vis DRS) were obtained by a UV-3600 diffuse reflectance spectroscopy. Particle size of all the materials were collected at ambient temperature on an Andon paar (Litersizer500) dynamic light scattering (DLS) annlyzer. Steady-state photoluminescence (PL) emission spectra and PL decay spectra

were measured at room temperature using a QM/TM fluorometer with the excitation wavelength of 365 and 386 nm, respectively. Scanning electron microscope (SEM) images were obtained on a Hitachi SU8010 microscope. Transmission electron microscope (TEM) characterizations were conducted using a Talos F200S microscope with an accelerating voltage of 200 KV. Specific surface area, pore volume, and pore size distribution data were obtained on a Micro ASAP 2046 surface area and porosity analyzer.

S2.1. Electrochemical measurements

Indium-tin oxide (ITO) glasses were firstly cleaned by sonication in ethanol for 30 min. 4 mg of samples power was mixed with 70 μL 5% Nafion and 1 mL *n*BuOH and ultra-sonicated for 60 min to get slurry. 120 μL of the slurry was spreading onto ITO glass and natural drying in air. A conventional three electrodes cell was used with a platinum mesh as the counter electrode and an Ag/AgCl electrode (saturated KCl) as reference electrode. The electrolyte was a 0.2 M Na_2SO_4 aqueous solution (pH=6.8) and was purged with nitrogen gas for 1 h prior to the measurements. The working electrodes were immersed in the electrolyte for 60 s before any measurements were taken. The photocurrent measurements were conducted with a GAMRY workstation, with the working electrodes irradiated from the front side. The visible light was generated by a 300 W xenon lamp (PerfectLight, PLS-SXE300/300UV) with a 400 nm cut-off filter, and was chopped manually. For Mott-Schottky experiments, the perturbation signal was 5 mV with the frequency of 1000, 2000 and 3000 Hz. The electrochemical impedance measurements were performed in dark at open-circuit voltage with AC amplitude of 5 mV in the frequencies range of 0.01 Hz to 10^5 Hz.[3] The applied potentials vs. Ag/AgCl are converted to RHE potentials using the following equation: $E_{RHE} = E_{Ag/AgCl} + 0.0591pH + E^{\theta}_{Ag/AgCl}$ ($E^{\theta}_{Ag/AgCl} = 0.199$ V).

S2.2. Photocatalytic hydrogen evolution measurements

Typically, 10 mg photocatalysts were loaded with 3.0 wt% Pt dispersed (chloroplatinic acid hexahydrate as precursor) into a 50 mL 1M aqueous ascorbic acid solution via ultrasonic treatment for 15 min under sealed environment. After that, the mixture was transferred into the closed gas circulation system (Perfect Light Company Labsolar-6A). The temperature of the reaction solution was maintained at 5 °C by the flow of cooling water. Prior to the photocatalytic test, the system was purged with Ar flow to remove air. A 300 W Xe lamp (Perfect Light PLS-SXE 300, 57 mW cm^{-1}) was used as the light source. The wavelength of the incident light was controlled by using a 400 nm long pass cut-off filter. The amount of H_2 evolved was determined using gas chromatography (SHIMADZU GC-2014, thermal conductivity detector (TCD), Ar carrier, Agilent). Hydrogen dissolved in the reaction mixture was not measured and the pressure increase generated by the evolved hydrogen was neglected in the calculations.

S2.3. Apparent quantum efficiency (AQE) measurements.

AQE measurements for hydrogen evolution were performed under the illumination of a 300 W Xe lamp with 410 nm band pass filters ($\lambda_0 \pm 20$ nm) for 4 hours. An optical diode power meter (FZ-A spectroradiometer) was used to measure its photon flux with an intensity of 3.5 mW cm^{-1}. For these tests, 30 mg of photocatalyst was used. The apparent quantum efficiency was calculated using the following formula:

$$AQE = \frac{N_e}{N_p} \times 100\% = \frac{2 \times M \times N_A}{\frac{E_{total}}{E_{Photon}}} \times 100\% = \frac{2 \times M \times N_A}{\frac{S \times p \times t}{h \times \frac{c}{\lambda}}} \times 100\% = \frac{2 \times M \times N_A \times h \times c}{S \times P \times t \times \lambda} \times 100\%$$

where Ne is the amount of generated electrons, Np is the incident photons, M is the amount of Hydrogen molecules (mol), N_A is Avogadro constant (6.022×10^{23} mol^{-1}), h is the Planck constant (6.626×10^{-34} J·s), c is the speed of light (3×10^8 m s^{-1}), S is the irradiation area (cm^2), P is the intensity of irradiation light (W cm^{-2}), t is the photoreaction time (s), λ is the wavelength of the monochromatic light (m).

S3. Supplementary Figures and tables

S3.1. Figures

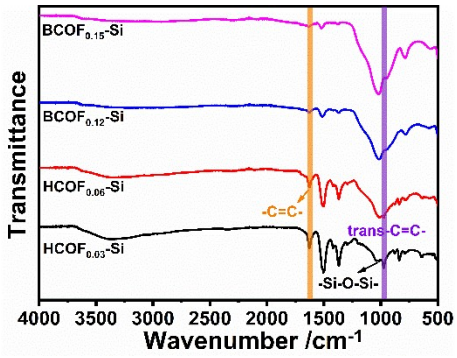

Fig. S1 FT-IR spectra of $HCOF_{0.03}$-Si, $HCOF_{0.06}$-Si, $BCOF_{0.12}$-Si, $BCOF_{0.15}$-Si.

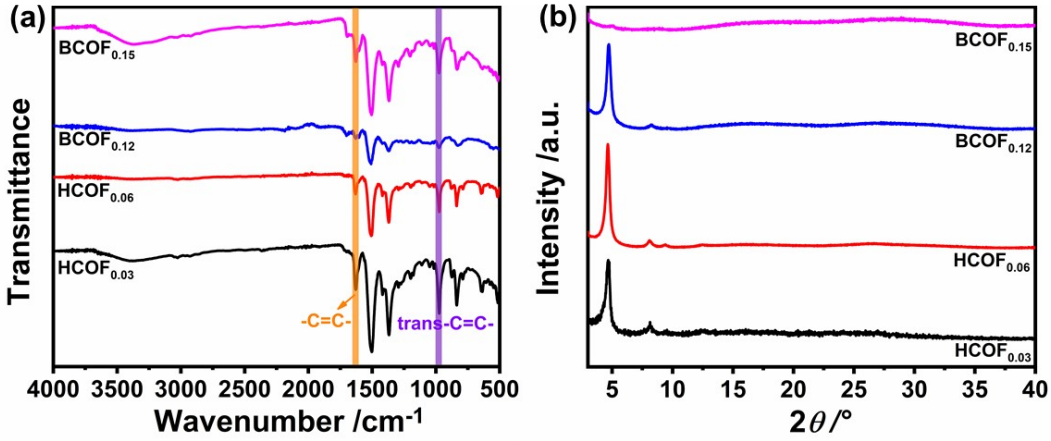

Fig. S2 (a) FT-IR spectra and (b) powder XRD patterns of $HCOF_{0.03,}$ $HCOF_{0.06}$, $BCOF_{0.12}$ and $BCOF_{0.15}$.

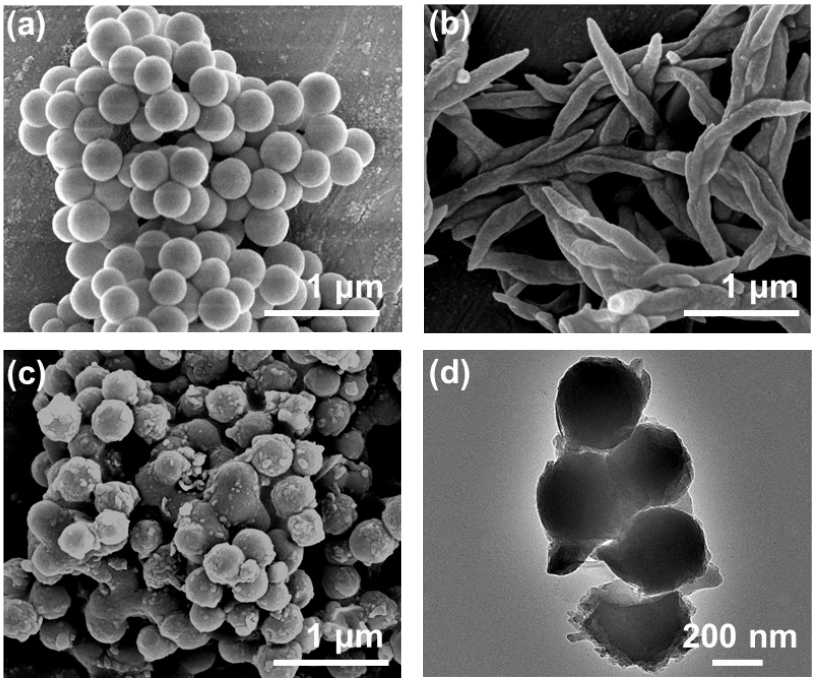

Fig. S3 SEM images of (a) NH_2-SiO_2, (b) pristine COF, (c) $HCOF_{0.09}$-Si, (d) TEM image of $HCOF_{0.09}$-Si.

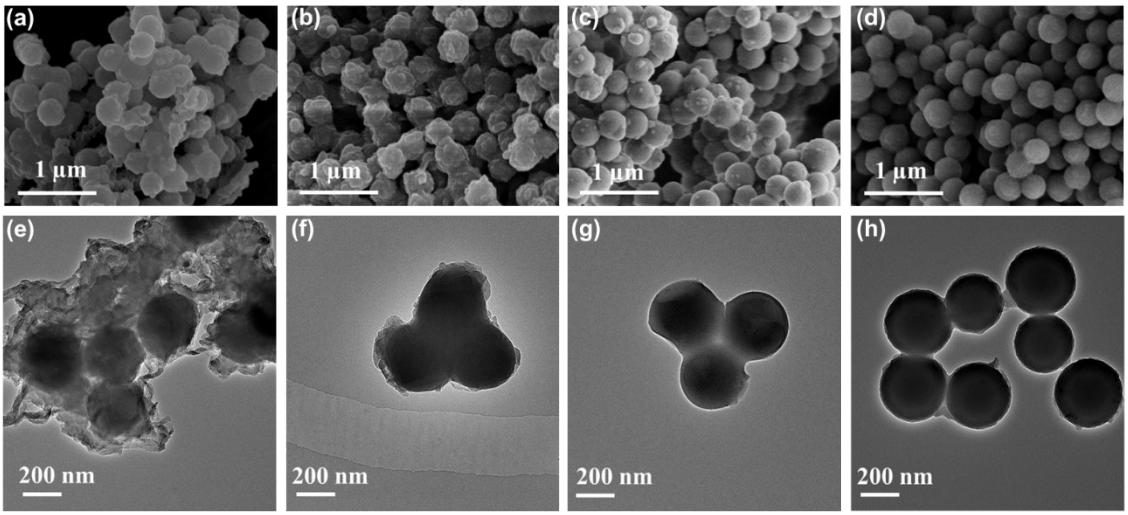

Fig. S4 SEM and TEM images of (a,e) $HCOF_{0.03}$-Si, (b,f) $HCOF_{0.06}$-Si, (c,g) $BCOF_{0.12}$-Si, (d,h) $BCOF_{0.15}$-Si.

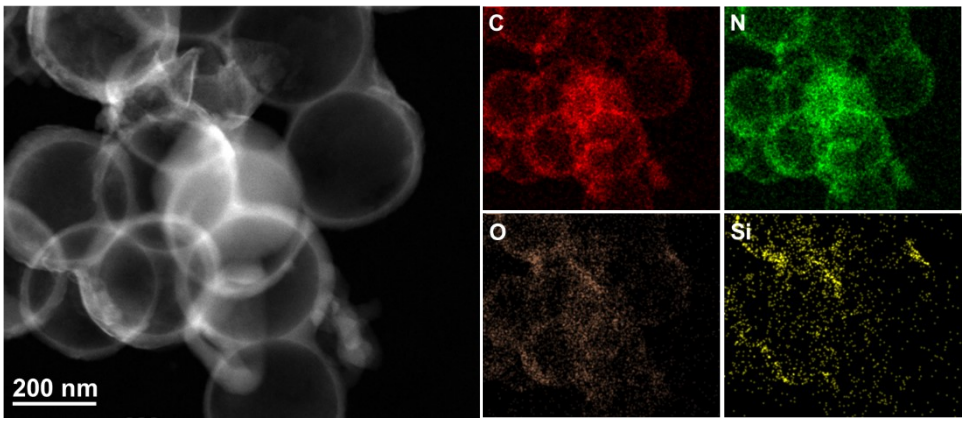

Fig. S5 TEM images and elements mapping of $HCOF_{0.09}$ with additional 24 h washing.

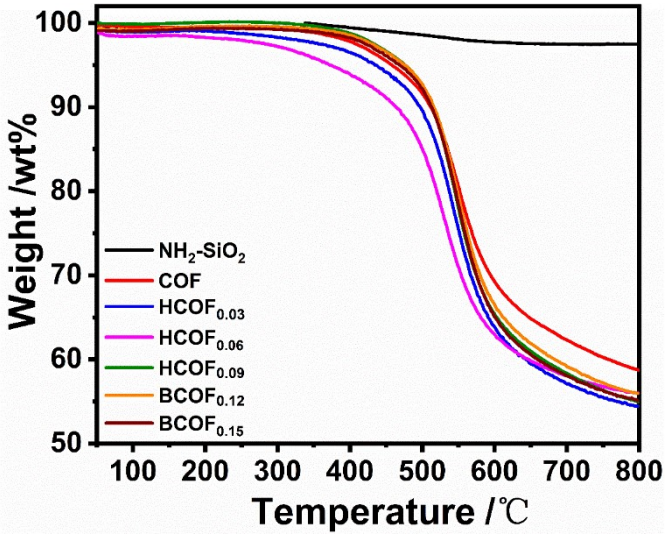

Fig. S6 TGA profiles of NH_2-SiO_2, pristine COF, $HCOF_{x1}$ and $BCOF_{x2}$.

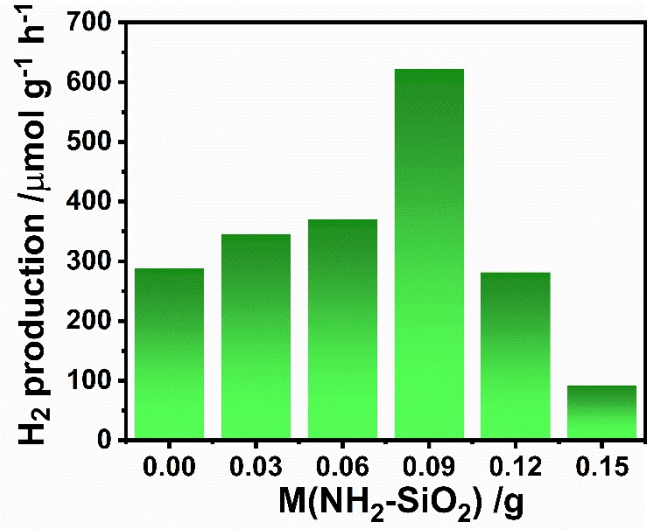

Fig. S7 H_2 evolution rate from water splitting with increasing amount of NH_2-SiO_2.

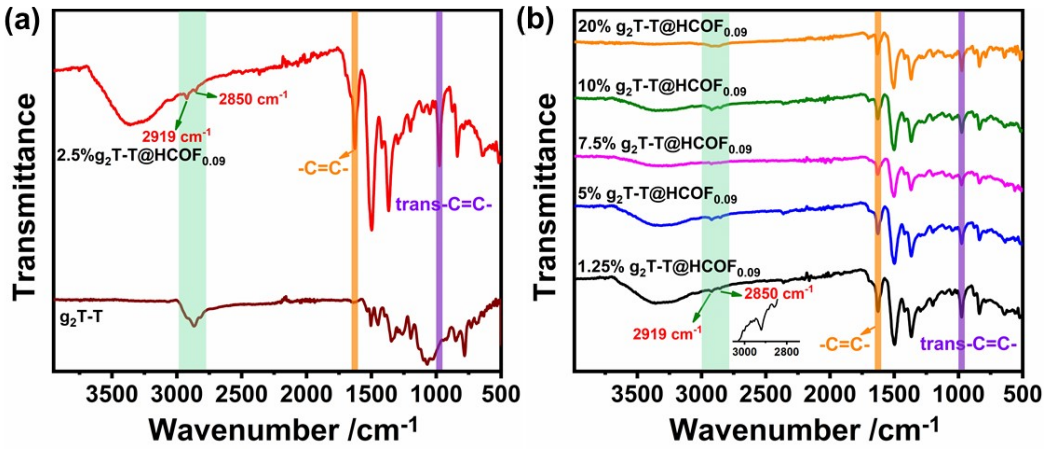

Fig. S8 FT-IR spectra of (a) g_2T-T and 2.5% g_2T-T@$HCOF_{0.09}$, (b) 1.25% g_2T-T@$HCOF_{0.09}$, 5% g_2T-T@$HCOF_{0.09}$, 7.5% g_2T-T@$HCOF_{0.09}$, 10% g_2T-T@$HCOF_{0.09}$, 20% g_2T-T@$HCOF_{0.09}$.

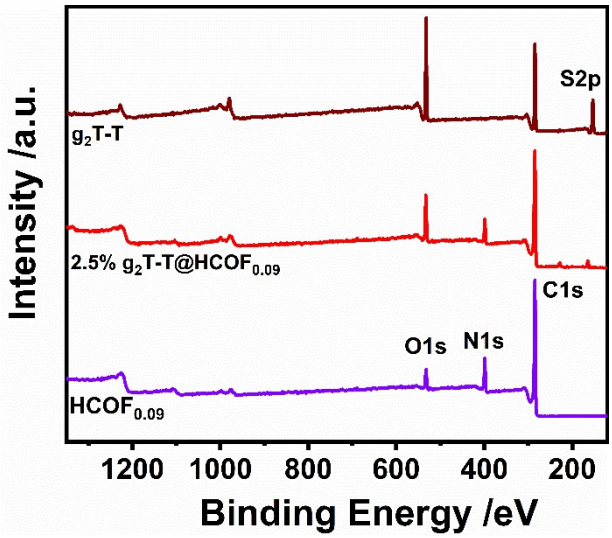

Fig. S9 Full survey XPS spectra of $HCOF_{0.09}$, 2.5% g_2T-T@$HCOF_{0.09}$ and g_2T-T.

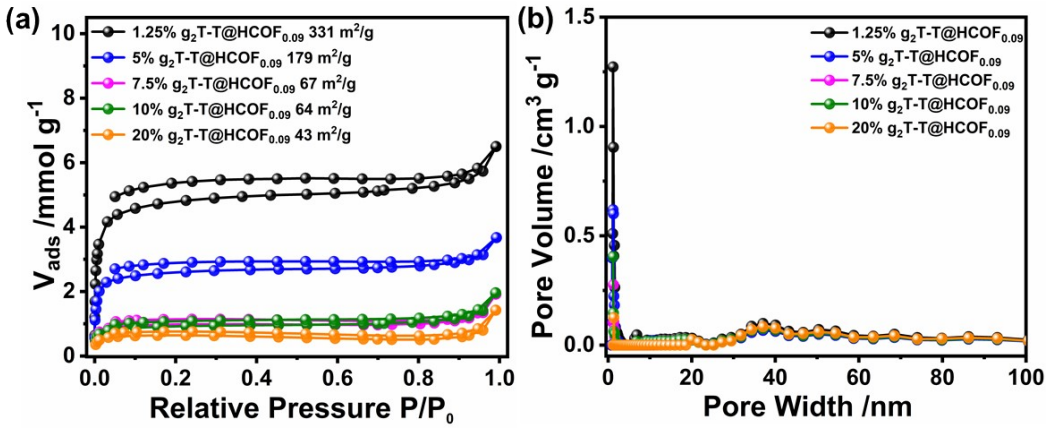

Fig. S10 (a) N_2 adsorption/desorption isotherms and (b) corresponding DFT pore size distributions of 1.25% g_2T-T@HCOF$_{0.09}$, 5% g_2T-T@HCOF$_{0.09}$, 7.5% g_2T-T@HCOF$_{0.09}$, 10% g_2T-T@HCOF$_{0.09}$, 20% g_2T-T@HCOF$_{0.09}$.

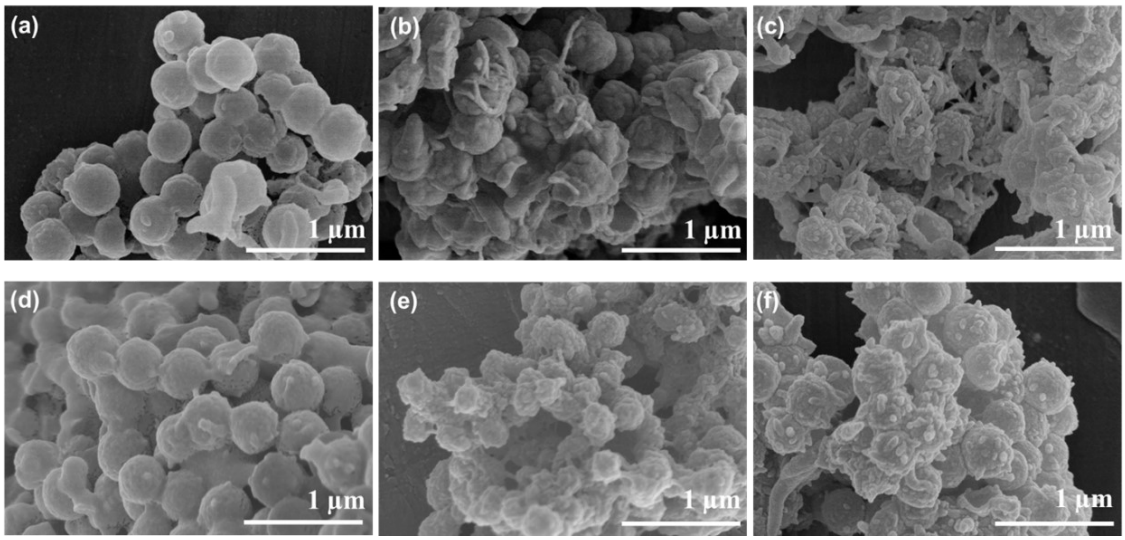

Fig. S11 SEM images of (a) 1.25% g_2T-T@HCOF$_{0.09}$, (b) 2.5% g_2T-T@HCOF$_{0.09}$, (c) 5% g_2T-T@HCOF$_{0.09}$, (d) 7.5% g_2T-T@HCOF$_{0.09}$, (e) 10% g_2T-T@HCOF$_{0.09}$, (f) 20% g_2T-T@HCOF$_{0.09}$.

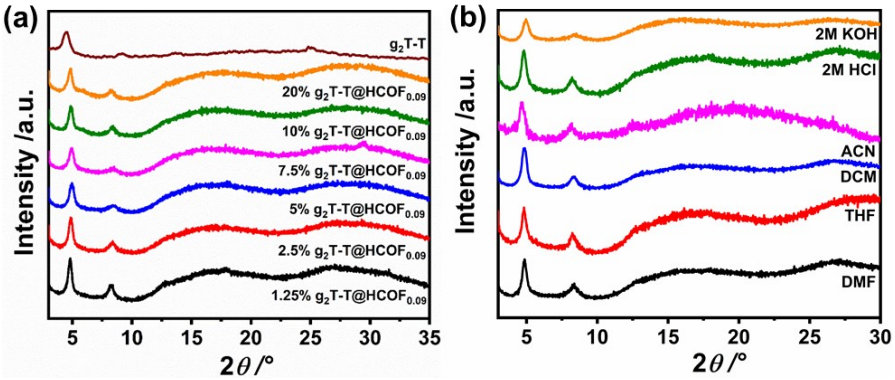

Fig. S12 PXRD patterns of (a) g_2T-T and y% g_2T-T@HCOF$_{0.09}$, (b) 2.5% g_2T-T@HCOF$_{0.09}$ immersed in different organic solvents, acid and base solutions for 72 h.

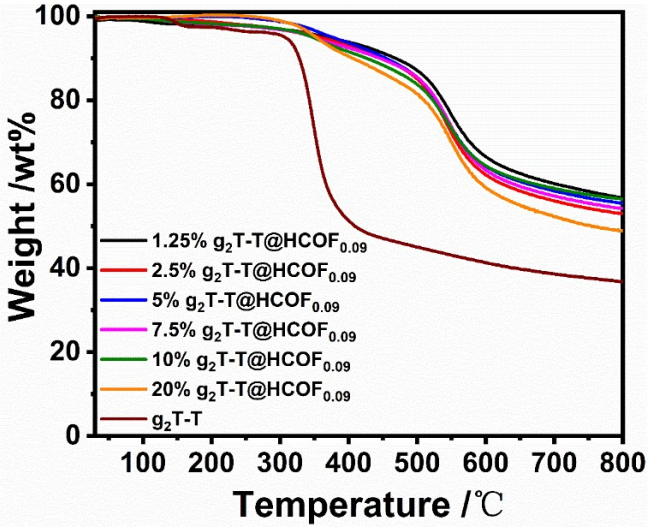

Fig. S13 TGA profiles of y% g_2T-T@$HCOF_{0.09}$ and g_2T-T.

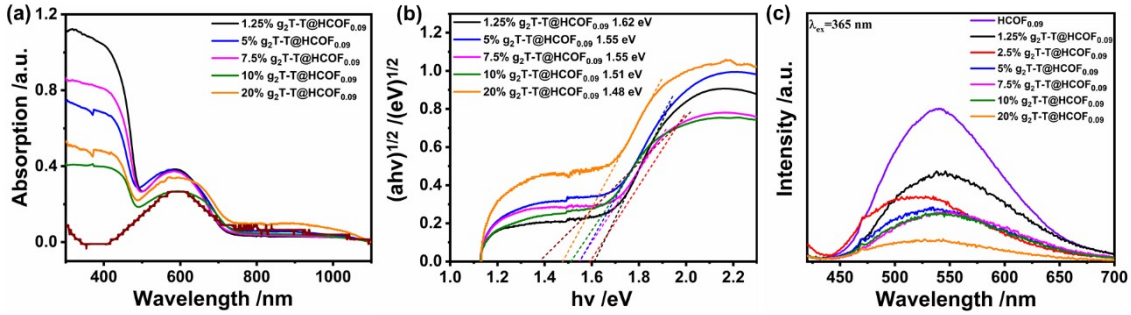

Fig. S14 (a) UV-vis DRS, (b) Tauc plots of y% g_2T-T@$HCOF_{0.09}$; (c) PL emission spectra (λ_{ex}=365 nm) of $HCOF_{0.09}$, y% g_2T-T@$HCOF_{0.09}$.

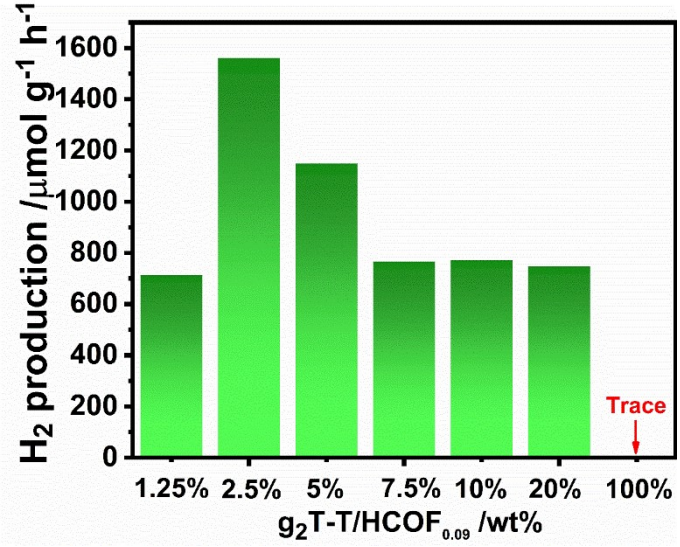

Fig. S15 H_2 evolution rate under visible-light irradiation with increasing amount of g_2T-T.

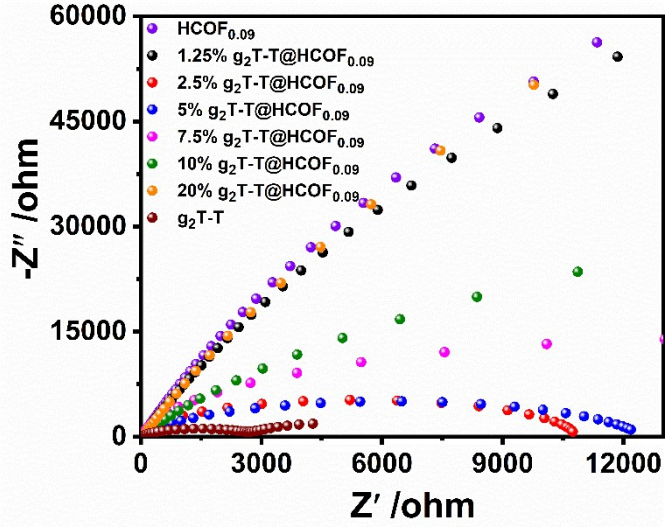

Fig. S16 Nyquist plots of $HCOF_{0.09}$, y% g_2T-T@$HCOF_{0.09}$, and g_2T-T.

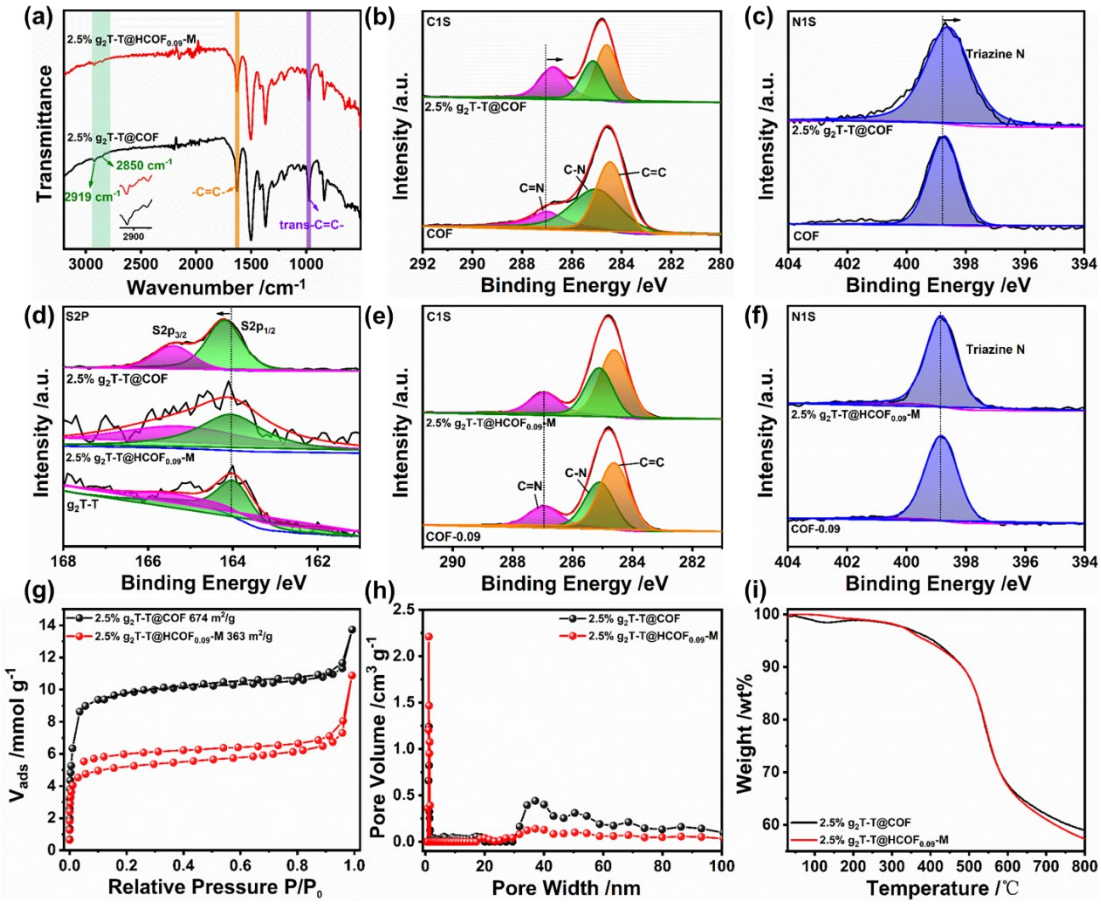

Fig. S17 (a) FT-IR spectra, (b,e) C1s core-level XPS spectra, (c,f) N1s core-level XPS spectra, (d) S2p core-level XPS spectra, (g) N_2 adsorption/ desorption isotherms, (h) corresponding DFT pore size distributions, (i) TGA profiles of pristine COF, 2.5% g_2T-T@COF and 2.5% g_2T-T@$HCOF_{0.09}$-M.

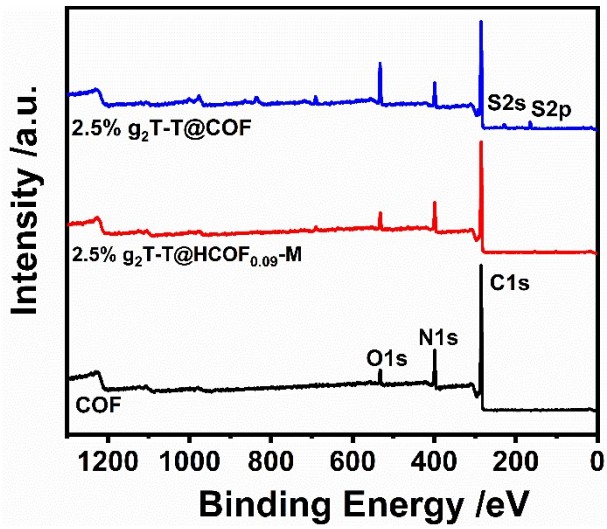

Fig. S18 Full survey XPS spectra of pristine COF, 2.5% g_2T-T@HCOF$_{0.09}$-M, and 2.5% g_2T-T@COF.

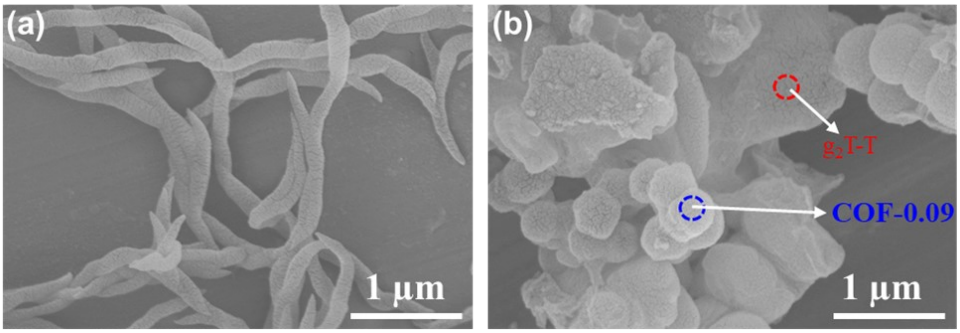

Fig. S19 SEM images of (a) 2.5% g_2T-T@COF, (b) 2.5% g_2T-T@HCOF$_{0.09}$-M.

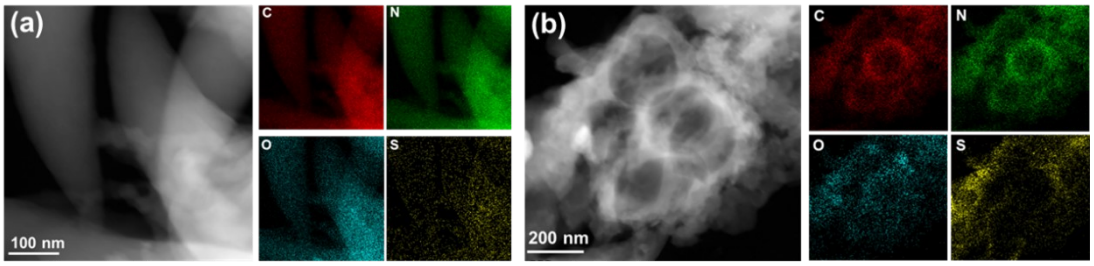

Fig. S20 TEM images and elements mapping of (a) 2.5% g_2T-T@COF, (b) 2.5% g_2T-T@HCOF$_{0.09}$-M.

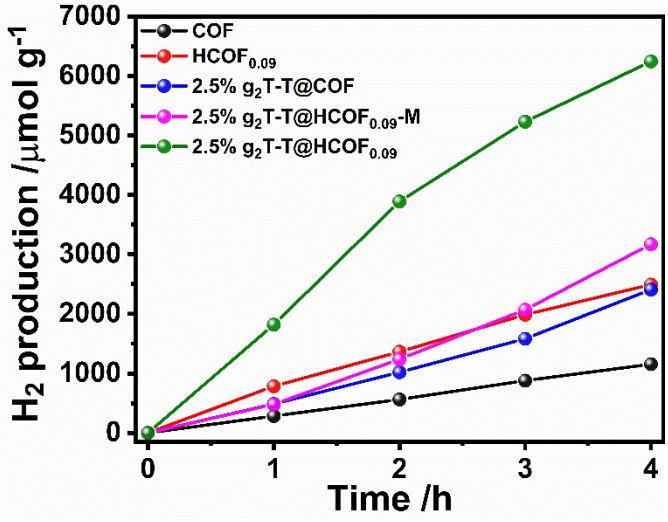

Fig. S21 Time courses of H_2 production of pristine COF, $HCOF_{0.09}$, 2.5% g_2T-T@COF, 2.5% g_2T-T@$HCOF_{0.09}$-M and 2.5% g_2T-T@$HCOF_{0.09}$.

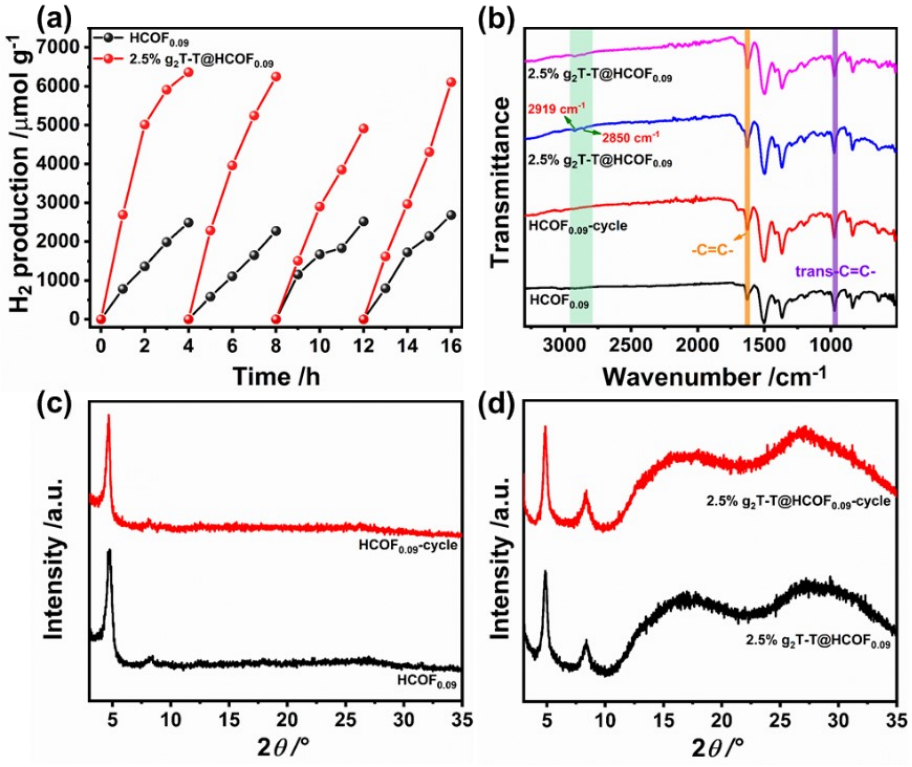

Fig. S22 Long-term photocatalytic tests: (a) H_2 generation behavior over time, (b) FT-IR spectra, (c,d) PXRD pattern.

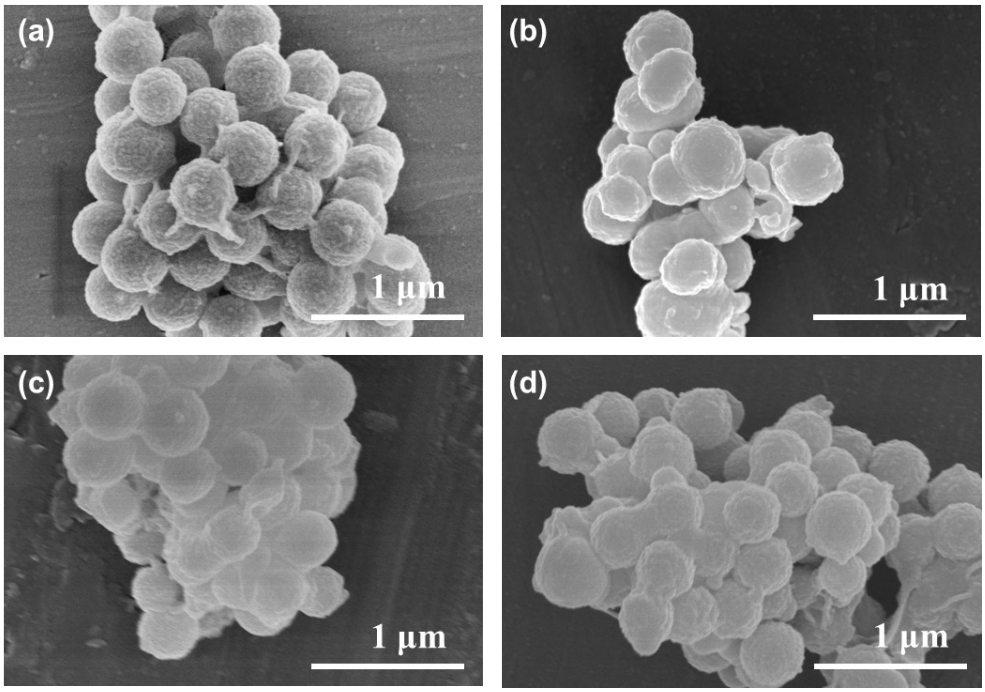

Fig. S23 SEM images of (a,c) $HCOF_{0.09}$ and 2.5% g_2T-T@$HCOF_{0.09}$; (b,d) $HCOF_{0.09}$ and 2.5% g_2T-T@$HCOF_{0.09}$ upon 16 hours cycling.

S3.2. Tables

Table S1 TEM elements analysis table of $HCOF_{0.09}$

Element	Atomic Fraction (%)	Atomic Error (%)	Mass Fraction (%)	Mass Error (%)	Fit error (%)
C	89.07	6.39	86.22	4.39	3.62
N	6.85	1.44	7.57	1.54	1.25
O	3.08	0.65	4.04	0.82	2.01
Si	1.01	0.21	2.17	0.43	1.46

Table S2 TEM elements analysis table of $HCOF_{0.09}$ with additional 24 h washing

Element	Atomic Fraction (%)	Atomic Error (%)	Mass Fraction (%)	Mass Error (%)	Fit error (%)
C	86.87	4.38	83.38	2.86	2.09
N	6.45	1.34	7.07	1.44	3.05
O	5.63	1.16	7.33	1.48	1.47
Si	1.05	0.21	2.22	0.43	2.04

Table S3 Summary of properties and H_2 evolution activity of vinylene-linked polymer-based visible-light photocatalytic systems

COF	Optical gap (eV)	Cocatalyst	H_2 evolution rate (μmol g^{-1} h^{-1})	References
2.5% g_2T-T@COF	1.59	3wt% Pt	1560	**This work**
60% COF-*o*OH	2.30	3wt% Pt	1119	[4]
60% COF-*m*OH	2.30	3wt% Pt	527	
60% COF-*p*OH	2.27	3wt% Pt	1302	
COF-alkene	3.87	3wt% Pt	2330	[5]
COF-imide	3.70	3wt% Pt	34	
COF-imine	3.85	3wt% Pt	12	
g-$C_{18}N_3$-COF	2.42	3wt% Pt	292	[1]
g-$C_{33}N_3$-COF	2.54	3wt% Pt	74	
g-$C_{40}N_3$-COF	2.36	3wt% Pt	2596	[6]
g-$C_{31}N_3$-COF	2.40	3wt% Pt	542	
g-$C_{37}N_3$-COF	2.52	3wt% Pt	396	
Sp^2C-COF	2.05	3wt% Pt	1360	[7]
Sp^2C-COF_{ERDN}	2.00	3wt% Pt	2120	
g-$C_{52}N_6$-COF	2.15	3wt% Pt	1178	[8]
CPN-3	2.27	3wt% Pt	1508	[9]
COF-DFB	2.3	3wt% Pt	2100	[10]
COF-BPDA	2.1	3wt% Pt	3230	
CBPP	2.22	25 mL	410	[11]
CBBP	2.20	PVP-Pt	840	
CFP	2.05	colloid	5070	
CBRP	2.15		470	
v-2D-COF-NS1	1.85	8wt% Pt	4400	[12]
v-2D-COF-NO1	1.86	8wt% Pt	1970	[13]
v-2D-COF-NO2	1.95	8wt% Pt	863	

Table S4 The band positions of $HCOF_{0.09}$ and g_2T-T

	g_2T-T	**$HCOF_{0.09}$**
Eg (eV)	1.37	2.25
E_{fb} (V vs. RHE)	1.58	-1.02
E_{CB} (eV vs. vacuum energy level)	-5.15	-3.72
E_{VB} (eV vs. vacuum energy level)	-6.52	-5.97

S4. Supplementary references

(1) S. Wei, F. Zhang, W. Zhang, P. Qiang, K. Yu, X. Fu, D. Wu, S. Bi and F. Zhang, *J. Am. Chem. Soc.,* 2019, **141**, 14272-14279.

(2) C. B. Nielsen, A. Giovannitti, D. T. Sbircea, E. Bandiello, M. R. Niazi, D. A. Hanifi, M. Sessolo, A. Amassian, G. G. Malliaras, J. Rivnay and I. McCulloch, *J. Am. Chem. Soc.,* 2016, **138**, 10252.

(3) J. Xie, C. Wang, N. Chen, W. Chen, J. Xu, P. Bai, L. Zhang and H. Wang, *J. Mater. Chem. C.,* 2021, **9**, 4378.

(4) C. Yang, C. Qian, M. Yu and Y. Liao, *Chem. Eng. J.,* 2023, **454**, 140341.

(5) C. Mo, M. Yang, F. Sun, J. Jian, L. Zhong, Z. Fang, J. Feng and D. Yu, *Adv. Sci.,* 2020, **7**, 1902988.

(6) S. Bi, C. Yang, W. Zhang, J. Xu, L. Liu, D. Wu, X. Wang, Y. Han, Q. Liang and F. Zhang, *Nat. Commun.,* 2019, **10**, 2467.

(7) E. Jin, Z. Lan, Q. Jiang, K. Geng, G. Li, X. Wang and D. Jiang, *Chem,* 2019, **5**, 1632-1647.

(8) J. Xu, C. Yang, S. Bi, W. Wang, Y. He, D. Wu, Q. Liang, X. Wang and F. Zhang, *Angew. Chem. Int. Ed.,* 2020, **59**, 23845-23853.

(9) Y. He, W. Ma, N. Yang, F. Liu, Y. Chen, H. Liu and X. Zhu, *Chem. Commun.,* 2021, **5**,7557-7560.

(10) S. Bi, F. Meng, D. Wu and F. Zhang, *J. Am. Chem. Soc.,* 2022, **144**, 3653-3659.

(11) S. Han, T. Huang, Y. Pan, J. Zhao, H. Lin, H. Lin, Z. Ding, H. Xi and J. Long, *Catal. Sci. Technol.,* 2021, **11**, 4021-4025.

(12) S. Li, R. Ma, S. Xu, T. Zheng, H. Wang, G. Fu, H. Yang, Y. Hou, Z. Liao, B. Wu, X. Feng, L. Wu, X. B. Li and T. Zhang, *ACS Catal.,* 2023, **13**, 1089-1096.

(13) S. Li, R. Ma, S. Xu, T. Zheng, G. Fu, Y. Wu, Z. Liao, Y. Kuang, Y. Hou, D. Wang, P. S. Petkov, K. Simeonova, X. Feng, Z. X. Wu, B. Li and T. Zhang, *J. Am. Chem. Soc.,* 2022, **144**, 13953-13960.